The structural basis of large-scale functional connectivity in the mouse

Draft for Journal of Neuroscience

Running title: *The structural basis of functional connectivity*

Authors: Joanes Grandjean [a,b*], Valerio Zerbi [c*], Joshua Balsters [c,d], Nicole Wenderoth [c,e**], Markus Rudin [a,e,f**]

[a] Institute for Biomedical Engineering, University and ETH Zurich, Wolfgang-Pauli-Str. 27, 8093 Zurich, Switzerland

[b] Singapore BioImaging Consortium, Agency for Science Technology and Research, 11 Biopolis Way, 138667 Singapore, Singapore

[c] Neural Control of Movement Lab, HEST, ETH Zürich, Winterthurerstrasse 190, 8057 Zurich, Switzerland

[d] Department of Psychology, Royal Holloway University of London, Egham, Surrey, UK.

[e] Neuroscience Center Zurich, University and ETH Zurich, Winterthurerstrasse 190, 8057 Zurich, Switzerland

[f] Institute of Pharmacology and Toxicology, University of Zurich, Winterthurerstrasse 190, 8057 Zurich, Switzerland

*Joanes Grandjean and Valerio Zerbi equally contributed to this manuscript and share first authorship

** Shared last authorship

Corresponding author:

Prof. Dr. Markus Rudin
Institute for Biomedical Engineering
University and ETH Zürich

AIC-ETH HCI D426
Vladimir-Prelog-Weg 4
CH- 8093 Zürich

Tel: +41 (0)44 633 76 04
Fax: +41 (0)44 633 11 87
e-mail: rudin@biomed.ee.ethz.ch

Pages: 25

Figures: 5

Abstract: 245 words, Introduction: 650 words, and Discussion: 1220 words

Conflict of Interest: The authors have no conflict of interest to declare.

Acknowledgements: This work was supported by the Swiss National Science Foundation (grant number 310030_141202 and 310030_160310 to MR), and the Swiss Foundation for Excellence and Talent in Biomedical Research (to MR). V.Z. is supported by ETH Career Seed Grant SEED-42 16-1.

Abstract

Translational neuroimaging requires approaches and techniques that can bridge between multiple different species and disease states. One candidate method, which offers insights into the brain's functional connectivity (FC), is resting state fMRI (rs-fMRI). In both humans and non-human primates, patterns of functional connectivity (often referred to as the functional connectome) have been related to the underlying structural connectivity (structural connectome). Given the recent rise in pre-clinical neuroimaging of mouse models it is an important question whether the mouse functional connectome conforms to the underlying structural connectivity. Here, we compared FC derived from rs-fMRI in mouse to the underlying monosynaptic structural connectome as provided by the Allen Brain Connectivity Atlas. We show that FC between inter-hemispheric homotopic cortical and hippocampal areas, as well as in cortical-striatal pathways, emerge primarily via monosynaptic structural connections. In particular, we demonstrate that the striatum can be segregated according to differential rs-fMRI connectivity patterns that mirror monosynaptic connectivity with isocortex. By contrast, for certain subcortical networks, FC emerges along polysynaptic pathways as shown for left and right striatum, which do not share direct anatomical connections, but high FC is putatively driven by a top-down cortical control. Finally, we show that FC involving cortico-thalamic pathways is limited, possibly confounded by the effect of anesthesia, small regional size and tracer injection volume. These findings provide a critical foundation for using rs-fMRI connectivity as a translational tool to study complex brain circuitry interactions and their pathology due to neurological or psychiatric diseases across species.

Significance statement

A comprehensive understanding of how the anatomical architecture of the brain, often referred to as the "connectome", corresponds to its function is arguably one of the biggest challenges for understanding the brain and its pathologies. Here we use the mouse as a model for comparing functional connectivity derived from resting-state fMRI with gold standard structural connectivity measures based on tracer injections. In particular, we demonstrate high correspondence between functional connectivity measurements of cortico-cortico and cortico-striatal and their anatomical underpinnings. This work provides a critical foundation for studying the pathology of these circuits across mouse models and human patients.

Keywords: Functional connectome, structural connectivity, mouse, viral tracer, resting-state fMRI

Introduction

The brain relies on finely tuned and adaptable neuronal networks for the control of perception, cognition, and behaviour. The organization of these networks at micro-, meso-, and macro-scale levels are considered essential to for the segregation and integration of information throughout the brain (Bullmore and Sporns, 2009; Park and Friston, 2013). Neuronal networks can be identified either at the structural level, i.e. represented by the physical presence of neuron cell bodies, dendrites, projecting axons, and synapses connecting two neuronal entities, or at the functional level, i.e. by dependencies of spiking and synaptic activities across neurons (Park and Friston, 2013). Such structural and functional measurements of the brain can then be conceptualised by describing regions-of-interest as nodes and interactions between nodes as edges, a framework that has become important for defining the intrinsic architecture of the brain - also referred to as “the connectome” - as well as it’s alterations due to disorders (Bullmore and Sporns, 2009). Information on the functional connectome can be resolved using resting-state functional magnetic resonance imaging (rs-fMRI). Rs-fMRI estimates the statistical interdependence of two brain areas from temporal correlations of fluctuating blood oxygen levels (Biswal et al., 1995; Damoiseaux et al., 2006; De Luca et al., 2006; Biswal et al., 2010). It has been proposed that high functional connectivity (FC) between remote brain areas results from information exchange via anatomical connections suggesting that emerging functional networks indirectly reflects the architecture of the structural connectome (Honey et al., 2009; van den Heuvel et al., 2009; Zhang et al., 2010). Several approaches are available to assess anatomical connectivity, such as *in-vivo* diffusion-weighted MRI (Basser et al., 1994) and tractography, as well as *ex-vivo* histological cyto-architectonic mapping (Kasthuri and Lichtman, 2007; Lichtman et al., 2008). For human studies, diffusion-weighted MRI-based connectome reconstruction has become the method of choice, being non-invasive and available in many research centers. However, tractography methods have difficulty resolving crossing-fibers (Jbabdi et al., 2015), they lose their sensitivity in gray matter and do not provide reliable information on track terminations. Anterograde/retrograde neuronal viral tracer studies in animal models are not hindered by crossing fibres, and are currently

considered the gold standard for determining monosynaptic axonal pathways (Swanson, 1982; Oh et al., 2014; Zingg et al., 2014; Hintiryan et al., 2016). Recently, viral tracers have been used to extensively map the mouse brain's monosynaptic structural connectome at the mesoscale level (Oh et al., 2014; Zingg et al., 2014; Hintiryan et al., 2016). This offers new opportunities to validate non-invasive imaging methods against the anatomical ground truth using a mammalian model, which shares several key principles of network architecture with the human brain (Stafford et al., 2014; van den Heuvel et al., 2016). However, in the past, detailed structure-function comparisons in the mouse brain have been limited by the achievable rs-fMRI quality. Here we used advanced MRI technology and protocols (Grandjean et al., 2014; Zerbi et al., 2015) for deriving the brain-wide functional connectome of mouse from high-resolution rs-fMRI acquisitions, which we then compared through a systematic approach with the monosynaptic structural connectome derived from viral tracings (Allen Brain Institute, http://connectivity.brain-map.org/).

Our results confirm that high FC emerges predominantly between monosynaptically connected regions. In addition to strong functional connectivity between homotopic areas of left and right isocortex, we show now for the mouse brain that the striatum can be segregated according to differential rs-fMRI connectivity patterns, which mirror monosynaptic structural connectivity with isocortex. Interestingly, we also found that high FC between subcortical structures of the left and right hemisphere emerges via polysynaptic pathways suggesting that isocortex might be an important relay area for mediating FC that extends beyond the monosynaptic structural connectome. By contrast, FC along cortico-thalamic pathways was limited, possibly confounded by the effect of anesthesia, region-of-interest (ROI) size and tracer injection volume. These results provide a critical foundation for future work that aims to test connectivity changes in mouse models of human diseases to reveal how brain connectivity is altered in pathological phenotypes.

Materials and Methods

Structural connectivity:

The structural connectivity matrix based on viral tracer injections was adapted from Oh el al. (Oh et al., 2014). Briefly, adeno-associated viral anterograde tracers containing genes encoding for enhanced green fluorescent protein were sterotactically injected at different sites in mice. Following the injection, 2 weeks were allowed for the protein expression before the animals were scarified, the brain extracted, sectioned, imaged with 2-photon microscope, reconstructed into 3D fluorescence maps, and transformed into a common reference space. The connectivity was determined from the injection site to the projections by quantifying the fluorescence locally for each region-of-interest, and normalizing it with the volume of injection, see for details (Oh et al., 2014).

Viral-tracer maps resampled at 100 μm^3 were obtained using the query form from the Allen Institute database (Allen Institute for Brain Science, http://connectivity.brain-map.org/). Individual experiments were selected as follows: carried in wild-type C57BL/6 and with injection volume ranging 0.0001 to 0.5 ul. The anatomical reference template was coregistered into the AMBMC MRI template resampled at 100 μm^3 (Australian Mouse Brain Mapping Consortium, http://www.imaging.org.au/AMBMC), using ANTS with greedy SyN transformation (Advanced Normalization Tools v2.1, http://picsl.upenn.edu/software/ants/). The viral-tracer maps, as well as the anatomical atlas were then converted into MRI space using the transformations estimated earlier, using radiological convention, which represents inverted left and right orientations.

We limited the scope of our analysis to the ontological ROI groups of the Allen atlas which were fully covered by the fMRI volume acquisition: the isocortex (isocortex), cortical sub-plate (CTXsp), hippocampal formation (HFP), striatum (STR), palladium (PAL) and thalamus (TH).

fMRI data acquisition and preprocessing:

Mouse multi-echo fMRI data are available online (central.xnat.org, project_ID: ME_fMRI_MOUSE). The rs-fMRI functional connectome maps are freely available for consultation (http://doi.org/10.5905/ethz-1007-59).

The C57BL/6 female mice (n=14) were used in this study. The experiment was performed following the Swiss federal guidelines for animal experimentation, and under a license from the Zürich cantonal veterinary office. Animals were caged in standard housing with food and water *ad libitum*, and kept in a 12h light and night cycle. In preparation for the measurements, anesthesia was induced with isoflurane 3.5% for 4 min in a 1:4 oxygen to air mix. The animals were endotracheally intubated, and positioned on a MR-compatible support. The animals were fixed with ear bars, and mechanically ventilated with a ventilator (CWE, Ardmore, USA), with 2% isoflurane. A cannula was placed in the tail vein for medetomidine, 0.05 mg/kg bolus followed 5 min later by 0.1 mg/kg/h infusion, and pancuronium, 0.2 mg/kg bolus followed by 0.4 mg/kg/h infusion. Following medetomidine bolus injection, isoflurane was reduced to 1.5%, and further reduced to 0.5% during infusion. Animal preparation and measurement took 45 min, all animals recovered fully following the measurements.

The dataset were acquired on a 9.4T Bruker scanner, equipped with a BGA-S gradient system, a volume coil for excitation and a 2x2 phased-array receiver-only cryogenic coil. Multi-echo gradient-echo EPI (ME-EPI) were acquired with the following parameters: repetition time 1500 ms, echo time [11, 17, 23] ms, flip angle 60°, matrix size 60x30, field of view 18.2x9 mm^2, number of slices 20, slice thickness 0.3 mm, slice gap 0.05 mm, 600 volumes, acceleration factor 1.4, horizontal field of view saturation slice to mask the lower portion of the mouse head, 250000 Hz bandwidth. Images presented minimal distortions, even at higher echo time.

ME-EPI were converted to NIFTI format and processed with meica.py script (AFNI_2011_12_21_1014, http://afni.nimh.nih.gov) (Kundu et al., 2012). Briefly, the script performs motion correction, despiking, skull stripping, and an ICA decomposition of the 3 echo-separated 4D images. Echo-time dependency is measured in each component and used to discriminate BOLD-related from non-BOLD related components. Components that did not

present echo-time signal dependency, i.e. non-BOLD, were labeled as noise are then regressed to obtain a final denoised 4D image. The denoised fMRI images were then co-registered to the MRI template using linear affine and non-linear greedy SyN transformation. We identified large scale FC networks using an independent component analysis (group-ICA MELODIC, FMRIB Software Library v5.0, http://fsl.fmrib.ox.ac.uk) as a tool to evaluate the quality of the cleaned data. Of the 30 predetermined components, 17 were representing known cortical and subcortical networks with plausible anatomical locations (Figure 1), based on definitions outlined in (Zerbi et al., 2015). Other components displayed spatial maps with irregular clusters not related to anatomical gray matter structures. None of the components related to motion or to vascular structures have been found. This is in line with previous observations using similar acquisition protocols, but different artifact cleaning methods (Zerbi et al., 2015). Seed-based maps were computed in FSL with the GIm function, using the viral injection site and injection volume to define the 238 rs-fMRI seeds. FC between each seed and the 254 target regions taken from the Allen reference atlas with the same ontology as used in Oh et al.(Oh et al., 2014) was calculated using Pearson's correlation and Fisher-Z transformed. Individual z-statistic seed-to-target matrices were pre-masked using a t-test to consider only connections significantly different than 0 (p=0.05, FDR corrected) and group averaged. The correlation between the SC and FC in each individual tracer experiment (i.e. each row in the connectome matrices) was defined by partial Spearman's correlations that include region volume as a covariate in order to compensate the common dependency between both tracer-based connectivity and resting-state fMRI with regional target volumes (Sethi et al., 2017). The results yield values of no/weak [0-0.2], weak-to-moderate [0.2-0.4] and moderate-to-strong effect [0.4-0.6](Cohen, 1988). Nonparametric Spearman's correlation was used since we could not readily assume a linear relationship between tracer projection intensity and functional connectivity. In complement to the previous analysis with partial Spearman's correlation analysis using region volume as covariate, , receiver operatic characteristic (ROC) curves were computed as in (Calabrese et al., 2015), in order to define the gross agreement between anatomical macro-scale FC and SC. Briefly, SC and FC sub-matrices were selected from their

anatomical parent structures, log-transformed, normalized between zero and one and binarized using a series of 1000 thresholds to keep the 0–100% of connections. The resulting binary connectivity matrices were compared using receiver operatic characteristic (ROC) analysis with tracer-based connectivity as ground truth. The True Positive Rate and False Positive Rate vectors were plotted against each other and the resulting area under the curve (AUC) is used as measure of connectivity similarity between the two metrics. The AUC results were then compared against a null distribution of the same datasets using permutation testing. Permutation testing (1000 iterations) consisted of shuffling the labels of the FC sub-matrices. In each permutation, the total volume of brain covered by the labels was therefore identical between SC and FC, which excludes volume-based biases in the resulting values.

For every voxel within each mask (right hemisphere isocortex, left hemisphere striatum, and left thalamus) we extracted the transformed connectivity values for each injection site. This gave each voxel a connectivity profile indicating how strong or weak connectivity was at that voxel for each injection site, both for resting state fMRI and tracer connectivity. In order to determine whether resting state connectivity patterns matched those seen with tracer injections, we performed a winner-takes-all analysis labeling each voxel as belonging to the network with the largest connectivity value for a set of 20 injection sites distributed on the right isocortical hemisphere, as carried in Oh el al. (2014). In order to determine whether voxels showed the same connectivity fingerprint using resting state fMRI and tracers (i.e. voxels showed connectivity profile for injection sites in both modalities) we used Spearman's rho to correlate connectivity profiles at each voxel. False discovery rate (FDR, $p<0.05$) was used to correct for multiple comparisons.

Mono- and polysynaptic dependency connections were derived from a graph-theory approach. To this end, we used the symmetrical SC matrix (81×81, for ROI list see Table S1) adapted from Oh et al. (Oh et al., 2014). Symmetrical FC matrix was obtained by estimating the Pearson's correlation coefficient between the time series extracted from rs-fMRI scans using the same ROI set as for SC. Individual FC matrices were groups averaged without applying

any pre-masking to maintain its original distribution. Both symmetrical matrices were normalized to range 0 to 100. Connectivity matrices were binarized using varying threshold 0 to 100 by 1 increment, at each threshold level the minimal distance separating every ROI pair was estimated using igraph in R (The R Foundation for Statistical Computing, Vienna, Austria). For every threshold level, the interaction between each ROI pair were classified into three categories based on both SC and FC distance matrix: (i) monosynaptic FC ($distance_{SC}$=1 edge and $distance_{FC}$=1 edge); (ii) polysynaptic FC ($distance_{SC}$>1 edge and $distance_{FC}$=1 edge); and (iii) mismatch ($distance_{SC}$=1 edge and $distance_{FC}$>1 edge). The connectivity likelihood for each category was established as the incidence for each threshold level.

Results

Overlapping structural and functional connectivity in the mouse brain.

SC and FC represent different metrics that depict large-scale neuronal architecture. Viral-tracer distributions obtained from the Allen Brain Institute database and rs-fMRI seed-maps corresponding to the injection sites were normalized into common spatial coordinates. Voxel-wise representation of the viral-tracer distribution and seed-based FC for four selected injection sites/seeds provide a qualitative representation of the similarities and differences between SC and FC (Figure 2). For instance, tracer injected into the primary somatosensory area of the barrel field (SSp-bfd) highlighted projections to both ipsi- and contralateral barrel field and to motor cortex areas, as well as projections to ipislateral dorsal striatum and thalamus. Seed-based FC revealed a similar pattern, but included marked FC between both ipsi- and contralateral hemispheres of the dorsal striatum, and an absence of detectable FC to the thalamus. For injection sites in the motor (MOs) or anterior cingulate area (ACAv), striking overlaps between SC and FC were found. In both instances, the regions displaying high FC extending beyond those being monosynaptically connected, and included larger areas of the primary somatosensory cortex in the case of the MO seed, and of the retrosplenial area in the case of the ACAv seed. Finally, an injection site/seed in the dentate gyrus (DG) revealed SC

confined to the hippocampus, while the corresponding FC area extended across hippocampus, cingulate, retrosplenial, ecto-, endo-, and perirhinal cortical areas, elements of the putative rodent default-mode network (DMN) (Lu et al., 2012; Sforazzini et al., 2014a). This indicates that FC between some areas, in particular homologous cortical regions of the left and right hemisphere, emerges due to direct monosynaptic connections, whereas FC in spatially extended networks (e.g. DMN) indexes indirect polysynaptic connections.

In order to perform a comparison at a whole brain level, we used total monosynaptic connectivity matrices reconstructed using 238 viral tracer maps (Oh et al., 2014), and matched them to seed-based FC. Injection sites were located in the isocortex (n=98), hippocampal formation (HPF, n=39), cortical subplate (CTXsp, n=6), striatum (STR, n=33), pallidum (PAL, n=8) and thalamus (TH, n=54) (for ROI list, see Table S1). Ipsilateral and contralateral target regions (n=254) were selected from the Allen Institute mouse brain parcellation atlas (http://atlas.brain-map.org). Connectivity patterns found in the tracer injection-based SC matrix and in the seed-based FC matrices (Figure 3a,b) confirmed the observations made using voxel-wise maps; they exhibit marked similarities for cortical injection sites, showing high SC and FC with ipsi- and contralateral isocortex, as well as with ipsilateral sub-cortical structures (striatum, pallidum, cortical sub-plate). However, for other specific connections, as between isocortex and thalamus, FC is mostly absent despite dense monosynaptic connections. Regarding the hippocampal formation, strong SC is observed between injection sites located in the entorhinal cortical area toward the isocortical and sub-cortical structures except for the thalamus on both the ipsi- and contralateral side. This pattern was however not observed in the FC matrix. Partial Spearman's rank tests confirmed the general good agreement between FC and SC for most of the selected seeds (figure 3c). In the isocortex, intermediate-to-strong correlations (rho = 0.4-0.6) were found with the exception of prefrontal areas (anterior cingulate, prelimbic, infralimbic and orbitofrontal areas). Conversely, most of the seed-experiments of the thalamus showed null or weak effects (rho = 0-0.2) apart from of the ventral posteromedial nuclei (see supplementary figure 1). Interestingly, the degree of correlation

between the SC and FC metrics were strongly significantly correlated with the amount of viral tracer injected in the structural experiments ($p<0.001$).

The degree of similarities between SC and FC in the two metrics was further assessed within- and between-ontological structures by receiver operating characteristic (ROC) analysis (Fig 3d,e,f, Table S2). Area under the curve (AUC) estimated from the ROC analysis recapitulates the observation described above. In particular, significant correspondence exists between the isocortex injection sites/seeds and contralateral isocortex (Fig 3d, AUC=0.702), as well as between isocortex and striatum (Fig 3e, AUC=0.709). For connections between thalamus and isocortex, correspondence between FC and SC was low albeit significantly different from the null (i.e. chance level) distribution (Fig 2f, AUC=0.587) for both directionalities.

These three relevant large-scale connections were further analyzed at a voxel-level, for mapping the most strongly connected subareas of contralateral isocortex, striatum and thalamus. The hippocampal formation was not included in the detailed analysis as most of the structural projections from the hippocampus were found to be confined to this brain region (Figure 3a,b).

Similar modular organization of the structural and functional connectome in the Mouse cortex

Mammalian brains are organized into distinct large-scale structures also referred as sub-networks or modules (Bullmore and Sporns, 2009; Oh et al., 2014; Zingg et al., 2014; Liska et al., 2015). The combination of structural and functional connectivity information in the same analysis space provides two independent metrics for comparing the modular organization of the brain. A winner-takes-all approach from 20 selected cortical injection seeds (Figure 4a) revealed a remarkable correspondence between structural (Figure 4b, left panel) and functional modular architecture (Figure 4b, middle panel) in both the ipsi- and contralateral isocortex. In both metrics, the somatosensory motor cortex is divided into three distinct

modules, encompassing motor (red), sensory (green) and medial orbital (yellow) areas. A temporal associative module (light/dark blue) was found to encompass auditory and visual cortices as well as retrohippocampal regions such as the entorhinal cortex. Regions analogous to the DMN were highlighted, in particular the cingulate, prefrontal, and retrosplenial cortices (violet). This modular organization is consistent with sub-networks presented in previous viral tracer studies (Oh et al., 2014; Zingg et al., 2014). This data extend previous rs-fMRI work, in which the parcellation of the mouse brain produced only two cortical modules, lateral cortical network encompassing limb and barrel field modules, and DMN which included the temporal associative module found in this study (Liska et al., 2015).

Although the isocortex has a modular organization, it is likely that voxels (particularly voxels on the borders between modules) are not exclusively interconnected with only one module. In order to compare structural and functional connectivity fingerprints we created a connectivity profile for each voxel within a mask (strength of connectivity for each injection site/seed (n=98)). We then used Spearman's rho to correlate the structural and functional connectivity profile at each voxel, using the data from all the isocortical seed-experiments (n=98) and correcting for multiple comparisons using false discovery rate (FDR, $p<0.05$). This analysis highlights whether a target voxel has the same pattern of high and low connectivity for each tracer injection site, and whether these connectivity patterns are the same between SC and FC metrics. This analysis revealed that 86.9% of all voxels within contralateral isocortex survived FDR correction, demonstrating the high degree of overlap in connectivity fingerprints between SC and FC. Specifically, the structure-function relationship was strongest in the motor and medial orbital modules and in the DMN, while correlations were weaker in the area in between the sensory and the temporal associative module (Figure 4b, right panel).

Matching structural and functional topographies of the cortico-striatal pathways

Cortico-striatal projections are essential components of forebrain circuits widely involved in goal-directed behavior and motivation (Ferguson et al., 2011; Kozorovitskiy et al., 2012; Farrell et al., 2013). Hypo- or hyperactivity in these connections is associated with several

neuropsychiatric disorders, including autism and schizophrenia (Shepherd, 2013; Ferenczi et al., 2016). From an anatomical and functional perspective the striatum is clustered into distinct domains according to input and output regions (Choi et al., 2012; Jung et al., 2014). Winner-takes-all topographical maps confirmed such a modular organization in both structural and functional datasets, which appears divided into five macro-areas densely connected with cingulate areas (violet), motor (red), sensory (green), medial orbital (yellow) and temporal associative (blue) cortices (Figure 4c). The partition of the ipsilateral striatum presented remarkable similarities with modular divisions found with viral tracers (Oh et al., 2014; Hintiryan et al., 2016). Remarkably, 87.8% of striatal voxels showed a significant Spearman's correlation between anatomical and functional architecture, with the highest degree of correlation found in the motor cortex to dorsal striatum pathway.

Lack of FC for networks involving the thalamus

The thalamus is a highly heterogeneous structure, subdivided into distinct nuclei that are connected to the cerebral cortex through multiple anatomical loops and that process sensory, limbic, and heteromodal information (Behrens et al., 2003). Detailed maps of human and rodent cortico-thalamic cytoarchitecture are available (Jones, 2007; Oh et al., 2014). In humans, imaging data suggests an overall correspondence between structural diffusion data and functional imaging, albeit this has been only demonstrated at the macroscale level (Zhang et al., 2010). Our results revealed minimal correspondence of FC and SC between isocortex and ipsilateral thalamus. Statistically, only 8.8% of all voxels within the ipsilateral thalamus showed a significant overlap of connectivity profiles (Figure 4d). Specifically, these areas of good correspondence reflect the connections between the anteroventral nuclei of the thalamus with retrosplenial cortex (purple), and between the ventral posteromedial nuclei with somatosensory-barrel field cortex (green). For all the other nuclei, the overall structural monosynaptic connections derived from viral tracing were not reflected by the functional data as measured with rs-fMRI.

Mono- and polysynaptic dependency of resting-state networks

Our comparison of the SC and FC matrices revealed areas of similarities and divergences between the two connectivity measures. In a final set of analyses, we determined the minimum number of edges, or connections, separating two nodes (regions-of-interest). This analysis was run for both structural and functional connectivity matrices. The number of edges necessary to connect two nodes was used to divide structural-functional connectivity relationships into three categories: (i) monosynaptic FC; (ii) polysynaptic FC; and (iii) low FC despite monosynaptic SC, which were labelled 'mismatched'.

The two distance metrics showed a similar distribution. For low threshold values, most of the ROIs were found separated by 1 or 2 edges (Figure 5a,b). As expected, the distance between node pairs increased with higher threshold values, consistent with increasing sparsity of the matrices. High monosynaptic FC likelihood values were obtained between isocortex to the ipsilateral hippocampal formation and striatum (Figure 5c). Notably, high interhemispheric monosynaptic connectivity likelihood was also found between bilateral homotopic isocortices and, to a lesser extent, between hippocampal formations, as indicated by the plot restricted to contralateral homotopic ROIs (Figure 5c, left panel). Polysynaptic connectivity likelihood was found to be more diverse in terms of interactions between the ontological structures and hemispheres (Figure 5d). For instance, there were notable interhemispheric projections from the striatum towards the isocortex and the contralateral striatum, as well as between homotopic subcortical regions in both hemispheres (Figure 5d, left panel). In summary, we found that functional networks in the isocortex were predominantly monosynaptic. Sub-cortical networks, on the other hand, present more diverse projections, and rely in several instances on polysynaptic projections. Mismatched FC is mostly present in edges between thalamic and ROIs in the cortex, hippocampal formation, and striatum, consistent with the notions of weak thalamic FC observed above (Figure S2).

Discussion

Here we report the brain-wide functional connectome of mouse and analyze how circuits of enhanced long-range FC map onto monosynaptic structural pathways. We confirm that FC

emerges preferably along monosynaptic connections, for example between homotopic isocortical areas across hemispheres. We further show that rs-fMRI is an excellent tool for studying cortico-striatal subcircuits, which match monosynaptic anatomical connectivity. Lastly, we identified specific networks (for example high FC between left and right striatum and thalamus) where rs-fMRI oscillations synchronize via polysynaptic pathways.

Understanding the organizational principles underlying the structure-function relationship of the brain has been a central question in neuroscience. Converging evidence across species has confirmed fMRI measurements reflect neuronal activity, both for stimulus-evoked and resting-state fMRI (Logothetis et al., 2001; Mantini et al., 2007; Scholvinck et al., 2010). Moreover, the topology of human FC networks corresponds well to major structural tracts forming cortico-cortical (Hagmann et al., 2008; Honey et al., 2009; van den Heuvel et al., 2009), cortico-striatal (Jarbo and Verstynen, 2015) or cortico-thalamic (Zhang et al., 2010) circuits. However, many of these studies have been using information derived from diffusion weighted imaging to reconstruct SC networks. Unfortunately, there are still a number of limitations with diffusion imaging, including the limited spatial resolution, low sensitivity in gray matter, and difficulties with identifying of fiber crossings and terminations. Tracer information in the mouse, by contrast, allows one to reconstruct SC networks with greater spatial resolution, and without ambiguity with respect to fiber crossing or mono- and polysynaptic projections. Previous work comparing viral tracer to functional connectivity have, similarly to our work, reported systematically good correspondence between SC and FC, albeit these studies limited their scope to specific networks, either cortical networks (and specifically the default-mode network) (Stafford et al., 2014), or the hippocampus (Bergmann et al., 2016). We have been able to demonstrate structure-function correspondence using the proven hardwired connections between the nodes involved in a wide range of resting-state networks, many of which find correspondence with human networks (Sforazzini et al., 2014a).

Resting-state FC networks in humans and other species have shown a preponderant bilateral organization (Damoiseaux et al., 2006), with the exception of right and left fronto-parietal

networks in the human brain (van den Heuvel et al., 2009). Previous studies investigating resting-state networks in the rodent brain have also demonstrated this bilateral organization (Grandjean et al., 2014; Sforazzini et al., 2014a; Zerbi et al., 2015). A property lost or greatly reduced in mice presenting with agenesis of the corpus callosum, supporting the notion that axonal projections are causally involved in supporting distal FC (Sforazzini et al., 2014b; Schroeter et al., 2016). Many of these networks have been proposed to be analogous to human resting-state networks, such as the DMN and the salience network (Upadhyay et al., 2011; Lu et al., 2012; Sforazzini et al., 2014a). An interesting feature of rodent FC is the presence of robust striatal functional networks, which we have repeatedly found to be divided into three entities, the dorsal and lateral striatum mostly overlapping with the caudate and putamen, and ventral striatum overlapping with nucleus accumbens (Grandjean et al., 2014; Zerbi et al., 2015). This segregation into specific circuits is interesting because they are differentially affected in murine models of brain disorders related to substance abuse (Hyman et al., 2006), movement disorders (Poston and Eidelberg, 2012), major depression (Kerestes et al., 2015), Parkinson disease (Rolinski et al., 2015), and schizophrenia (Sorg et al., 2013) (for review, see (Shepherd, 2013)). One specific property of these networks is that in comparison to cortical networks, which rely strongly on direct projections, their bilateral organization relies on polysynaptic relays, either via the cortico-striatal or nigrostriatal/mesolimbic pathways (Ferenczi et al., 2016). Thus, the preponderant position of striatal networks among the rodent resting-state functional networks, and the availability of mouse models of brain disorders and substance abuse, offers new opportunities to study the large-scale functional implications of disease on these specific networks.

As well as highlighting the significant overlap between structural and functional connectivity, we also identified some networks where structural and functional connectivity did not match, specifically the cortico-thalamic projections. This might be attributed to effects of anesthesia. While controlled anesthesia and mechanical ventilation is expected to increase the robustness and reproducibility of the functional read-out by limiting drastically physiological noise through reduced motion and constant breathing cycle, anesthesia agents will also affect neuronal

networks. However, albeit kept to a minimal level, medetomidine has been reported to interfere with cortico-thalamic FC (Fukuda et al., 2013) particularly in connection to rs-fMRI studies (Grandjean et al., 2014; Nasrallah et al., 2014), specifically affecting regions expressing high levels of alpha-2 adrenergic receptors, the target of medetomidine, in a dose-dependent fashion (Nasrallah et al., 2014). Another possible confounding factor is the relatively small injection volume used to target the thalamic nuclei, an effect further exacerbated by the relative small ROI size of these corresponding nuclei. In fact, 22 out of 54 thalamic areas (41%) were injected with less than 0.1 µl of viral tracer. In comparison, only 28% of isocortical and 24% of striatal injections received less than 0.1µl of volume. The higher anatomically specificity obtained with small injections is desired for small nuclei such as in the thalamus. However, this is usually achieved at the cost of a reduced transcriptional efficiency of the virus and therefore a lower sensitivity of the measure; this may have introduced a systematic noise in the connectivity derived to macroscale ontological targets. Moreover, this effect is exacerbated by the relatively low resolution of fMRI, ~300µm^3, which does not permit to resolve smaller thalamic nucleus separately. Notably, our results showed a robust correlation between the SC - FC Spearman's rho and the injection volume, which corroborate these findings. Altogether this suggests that thalamic resting state networks in anesthetized rodents should be interpreted with caution, as their interpretation in terms of structural connectivity may be confounded by intrinsic shortcomings in the measurements.

The comparison between the two metrics remains limited in some aspects. First, in mouse studies anesthesia was shown to interfere with brain function and therefore to affect FC readouts as discussed for cortico-thalamic connectivity. Recent work has compared awake rs-fMRI to viral tracer, however, distal FC estimated in this latter work was relatively low with respect to the selected seeds (Bergmann et al., 2016) in comparison to results reported with the optimized anesthesia protocol used in this study (Grandjean et al., 2014). This corroborates previous reports indicating difficulties in adapting rat awake protocols to mice (Jonckers et al., 2014). In addition to displaying strong and robust distal FC, the anesthesia protocol was shown to recapitulate advantages of both isoflurane and medetomidine protocols, i.e. strong cortical

and sub-cortical FC respectively, while displaying minimal undesirable effects. Second, a study in monkey has shown that mild and deep anesthesia was associated with greater correspondence between FC and SC, while the awake state captured rich FC patterns beyond that predicted with anatomical projections, including patterns of dynamic FC (Barttfeld et al., 2015). While it remains difficult to compare anesthesia depth across studies and more so across species, the present study uses a light anesthesia/sedation protocol, which retains anti-correlation (Grandjean et al., 2014), and rich patterns of dynamic FC (Grandjean et al., 2017), comparable to results described in awake monkey. This may explain the presence of rich polysynaptic dependent FC observed in the present study. Third, tracer-based SC from the Allen Institute contains directional information between any two ROIs, whereas FC captured only the shared information between the time series, irrespective of the directionality. This may have biased the estimation of the correspondence between the two metrics, although recent studies showed a general good correspondence between anterograde and retrograde pathways in the mouse (Zingg et al., 2014). Indeed most anatomical projections are coupled with reciprocal projections which might offset directionality effect in the SC matrices. The hippocampus is a notable exception to this rule, as most projections are unidirectional and inputs to the hippocampus come exclusively from the parahippocampal formation, thus distal FC with respect to the hippocampus, such as with the other elements of the rodent DMN, is mostly exclusively polysynaptic dependent. Applying causal models such as Granger causality or dynamic causal modeling (Li et al., 2011) to resting-state networks may provide information regarding directionality and as such provide further information regarding the correspondence between structure and function.

Whole-brain comparison of SC estimated from tracer-based reconstruction and FC from rs-fMRI obtained in the mouse revealed substantial agreement between the two metrics across several levels from individual connectivity maps derived from injection sites/seeds, to whole-brain interactions, and to modular organization of FC/SC. This close correspondence between FC and SC forms the basis for linking resting-state fMRI in the mouse to its anatomical underpinnings, providing a strong foundation to investigate the structure/function relationship

as well as its alteration due to disease within networks. Our findings also form the basis for rodent fMRI in combination with pharmaco-/opto-genetically controlled manipulation to dissect the role of selected cellular populations in sub-networks (Lee et al., 2010), thus allowing to resolve cell-specific mechanism taking place in large-scale networks in the healthy and diseased brain. These approaches may shine new light onto the organization of the healthy brain, and onto specific neuronal alterations underlying brain disorders.

References:

Barttfeld P, Uhrig L, Sitt JD, Sigman M, Jarraya B, Dehaene S (2015) Signature of consciousness in the dynamics of resting-state brain activity. Proc Natl Acad Sci U S A 112:887-892.

Basser PJ, Mattiello J, LeBihan D (1994) MR diffusion tensor spectroscopy and imaging. Biophysical journal 66:259-267.

Behrens TE, Johansen-Berg H, Woolrich MW, Smith SM, Wheeler-Kingshott CA, Boulby PA, Barker GJ, Sillery EL, Sheehan K, Ciccarelli O, Thompson AJ, Brady JM, Matthews PM (2003) Non-invasive mapping of connections between human thalamus and cortex using diffusion imaging. Nature neuroscience 6:750-757.

Bergmann E, Zur G, Bershadsky G, Kahn I (2016) The Organization of Mouse and Human Cortico-Hippocampal Networks Estimated by Intrinsic Functional Connectivity. Cereb Cortex 26:4497-4512.

Biswal B, Yetkin FZ, Haughton VM, Hyde JS (1995) Functional connectivity in the motor cortex of resting human brain using echo-planar MRI. Magn Reson Med 34:537-541.

Biswal BB et al. (2010) Toward discovery science of human brain function. Proceedings of the National Academy of Sciences of the United States of America 107:4734-4739.

Bullmore E, Sporns O (2009) Complex brain networks: graph theoretical analysis of structural and functional systems. Nat Rev Neurosci 10:186-198.

Calabrese E, Badea A, Cofer G, Qi Y, Johnson GA (2015) A Diffusion MRI Tractography Connectome of the Mouse Brain and Comparison with Neuronal Tracer Data. Cereb Cortex 25:4628-4637.

Choi EY, Yeo BT, Buckner RL (2012) The organization of the human striatum estimated by intrinsic functional connectivity. J Neurophysiol 108:2242-2263.

Cohen J (1988) Statistical power analysis for the behavioral sciences. Hillsdale, N.J.: L. Erlbaum Associates.

Damoiseaux JS, Rombouts SA, Barkhof F, Scheltens P, Stam CJ, Smith SM, Beckmann CF (2006) Consistent resting-state networks across healthy subjects. Proc Natl Acad Sci U S A 103:13848-13853.

De Luca M, Beckmann CF, De Stefano N, Matthews PM, Smith SM (2006) fMRI resting state networks define distinct modes of long-distance interactions in the human brain. Neuroimage 29:1359-1367.

Farrell MS, Pei Y, Wan Y, Yadav PN, Daigle TL, Urban DJ, Lee HM, Sciaky N, Simmons A, Nonneman RJ, Huang XP, Hufeisen SJ, Guettier JM, Moy SS, Wess J, Caron MG, Calakos N, Roth BL (2013) A Galphas DREADD mouse for selective modulation of cAMP production in striatopallidal neurons. Neuropsychopharmacology : official publication of the American College of Neuropsychopharmacology 38:854-862.

Ferenczi EA, Zalocusky KA, Liston C, Grosenick L, Warden MR, Amatya D, Katovich K, Mehta H, Patenaude B, Ramakrishnan C, Kalanithi P, Etkin A, Knutson B, Glover GH, Deisseroth K (2016) Prefrontal cortical regulation of brainwide circuit dynamics and reward-related behavior. Science 351:aac9698.

Ferguson SM, Eskenazi D, Ishikawa M, Wanat MJ, Phillips PE, Dong Y, Roth BL, Neumaier JF (2011) Transient neuronal inhibition reveals opposing roles of indirect and direct pathways in sensitization. Nature neuroscience 14:22-24.

Fukuda M, Vazquez AL, Zong X, Kim SG (2013) Effects of the alpha(2)-adrenergic receptor agonist dexmedetomidine on neural, vascular and BOLD fMRI responses in the somatosensory cortex. Eur J Neurosci 37:80-95.

Grandjean J, Schroeter A, Batata I, Rudin M (2014) Optimization of anesthesia protocol for resting-state fMRI in mice based on differential effects of anesthetics on functional connectivity patterns. Neuroimage 102 Pt 2:838-847.

Grandjean J, Preti MG, Bolton TA, Buerge M, Seifritz E, Pryce CR, Van De Ville D, Rudin M (2017) Dynamic reorganization of intrinsic functional networks in the mouse brain. Neuroimage 152:497-508.

Hagmann P, Cammoun L, Gigandet X, Meuli R, Honey CJ, Wedeen VJ, Sporns O (2008) Mapping the structural core of human cerebral cortex. PLoS Biol 6:e159.

Hintiryan H, Foster NN, Bowman I, Bay M, Song MY, Gou L, Yamashita S, Bienkowski MS, Zingg B, Zhu M, Yang XW, Shih JC, Toga AW, Dong HW (2016) The mouse cortico-striatal projectome. Nat Neurosci 19:1100-1114.

Honey CJ, Sporns O, Cammoun L, Gigandet X, Thiran JP, Meuli R, Hagmann P (2009) Predicting human resting-state functional connectivity from structural connectivity. Proc Natl Acad Sci U S A 106:2035-2040.

Hyman SE, Malenka RC, Nestler EJ (2006) Neural mechanisms of addiction: the role of reward-related learning and memory. Annu Rev Neurosci 29:565-598.
Jarbo K, Verstynen TD (2015) Converging structural and functional connectivity of orbitofrontal, dorsolateral prefrontal, and posterior parietal cortex in the human striatum. J Neurosci 35:3865-3878.
Jbabdi S, Sotiropoulos SN, Haber SN, Van Essen DC, Behrens TE (2015) Measuring macroscopic brain connections in vivo. Nat Neurosci 18:1546-1555.
Jonckers E, Delgado YPR, Shah D, Guglielmetti C, Verhoye M, Van der Linden A (2014) Different anesthesia regimes modulate the functional connectivity outcome in mice. Magn Reson Med 72:1103-1112.
Jones EG (2007) The thalamus, 2nd Edition. Cambridge ; New York: Cambridge University Press.
Jung WH, Jang JH, Park JW, Kim E, Goo EH, Im OS, Kwon JS (2014) Unravelling the intrinsic functional organization of the human striatum: a parcellation and connectivity study based on resting-state FMRI. PloS one 9:e106768.
Kasthuri N, Lichtman JW (2007) The rise of the 'projectome'. Nature methods 4:307-308.
Kerestes R, Harrison BJ, Dandash O, Stephanou K, Whittle S, Pujol J, Davey CG (2015) Specific functional connectivity alterations of the dorsal striatum in young people with depression. Neuroimage Clin 7:266-272.
Kozorovitskiy Y, Saunders A, Johnson CA, Lowell BB, Sabatini BL (2012) Recurrent network activity drives striatal synaptogenesis. Nature 485:646-650.
Kundu P, Inati SJ, Evans JW, Luh WM, Bandettini PA (2012) Differentiating BOLD and non-BOLD signals in fMRI time series using multi-echo EPI. Neuroimage 60:1759-1770.
Lee JH, Durand R, Gradinaru V, Zhang F, Goshen I, Kim DS, Fenno LE, Ramakrishnan C, Deisseroth K (2010) Global and local fMRI signals driven by neurons defined optogenetically by type and wiring. Nature 465:788-792.
Li B, Daunizeau J, Stephan KE, Penny W, Hu D, Friston K (2011) Generalised filtering and stochastic DCM for fMRI. Neuroimage 58:442-457.
Lichtman JW, Livet J, Sanes JR (2008) A technicolour approach to the connectome. Nature reviews Neuroscience 9:417-422.
Liska A, Galbusera A, Schwarz AJ, Gozzi A (2015) Functional connectivity hubs of the mouse brain. Neuroimage 115:281-291.
Logothetis NK, Pauls J, Augath M, Trinath T, Oeltermann A (2001) Neurophysiological investigation of the basis of the fMRI signal. Nature 412:150-157.
Lu H, Zou Q, Gu H, Raichle ME, Stein EA, Yang Y (2012) Rat brains also have a default mode network. Proc Natl Acad Sci U S A 109:3979-3984.
Mantini D, Perrucci MG, Del Gratta C, Romani GL, Corbetta M (2007) Electrophysiological signatures of resting state networks in the human brain. Proc Natl Acad Sci U S A 104:13170-13175.
Nasrallah FA, Tay HC, Chuang KH (2014) Detection of functional connectivity in the resting mouse brain. Neuroimage 86:417-424.
Oh SW et al. (2014) A mesoscale connectome of the mouse brain. Nature 508:207-214.
Park HJ, Friston K (2013) Structural and functional brain networks: from connections to cognition. Science 342:1238411.
Poston KL, Eidelberg D (2012) Functional brain networks and abnormal connectivity in the movement disorders. Neuroimage 62:2261-2270.
Rolinski M, Griffanti L, Szewczyk-Krolikowski K, Menke RA, Wilcock GK, Filippini N, Zamboni G, Hu MT, Mackay CE (2015) Aberrant functional connectivity within the basal ganglia of patients with Parkinson's disease. Neuroimage Clin 8:126-132.
Scholvinck ML, Maier A, Ye FQ, Duyn JH, Leopold DA (2010) Neural basis of global resting-state fMRI activity. Proc Natl Acad Sci U S A 107:10238-10243.
Schroeter A, Grandjean J, Schlegel F, Saab BJ, Rudin M (2016) Contributions of structural connectivity and cerebrovascular parameters to functional magnetic resonance imaging signals in mice at rest and during sensory paw stimulation. J Cereb Blood Flow Metab.
Sethi SS, Zerbi V, Wenderoth N, Fornito A, Fulcher BD (2017) Structural connectome topology relates to regional BOLD signal dynamics in the mouse brain. Chaos: An Interdisciplinary Journal of Nonlinear Science 27:047405.
Sforazzini F, Schwarz AJ, Galbusera A, Bifone A, Gozzi A (2014a) Distributed BOLD and CBV-weighted resting-state networks in the mouse brain. Neuroimage 87:403-415.
Sforazzini F, Bertero A, Dodero L, David G, Galbusera A, Scattoni ML, Pasqualetti M, Gozzi A (2014b) Altered functional connectivity networks in acallosal and socially impaired BTBR mice. Brain Struct Funct.
Shepherd GM (2013) Corticostriatal connectivity and its role in disease. Nature reviews Neuroscience 14:278-291.

Sorg C, Manoliu A, Neufang S, Myers N, Peters H, Schwerthoffer D, Scherr M, Muhlau M, Zimmer C, Drzezga A, Forstl H, Bauml J, Eichele T, Wohlschlager AM, Riedl V (2013) Increased intrinsic brain activity in the striatum reflects symptom dimensions in schizophrenia. Schizophr Bull 39:387-395.

Stafford JM, Jarrett BR, Miranda-Dominguez O, Mills BD, Cain N, Mihalas S, Lahvis GP, Lattal KM, Mitchell SH, David SV, Fryer JD, Nigg JT, Fair DA (2014) Large-scale topology and the default mode network in the mouse connectome. Proceedings of the National Academy of Sciences of the United States of America 111:18745-18750.

Swanson LW (1982) The projections of the ventral tegmental area and adjacent regions: a combined fluorescent retrograde tracer and immunofluorescence study in the rat. Brain research bulletin 9:321-353.

Upadhyay J, Baker SJ, Chandran P, Miller L, Lee Y, Marek GJ, Sakoglu U, Chin CL, Luo F, Fox GB, Day M (2011) Default-mode-like network activation in awake rodents. PLoS One 6:e27839.

van den Heuvel MP, Bullmore ET, Sporns O (2016) Comparative Connectomics. Trends Cogn Sci.

van den Heuvel MP, Mandl RC, Kahn RS, Hulshoff Pol HE (2009) Functionally linked resting-state networks reflect the underlying structural connectivity architecture of the human brain. Hum Brain Mapp 30:3127-3141.

Zerbi V, Grandjean J, Rudin M, Wenderoth N (2015) Mapping the mouse brain with rs-fMRI: An optimized pipeline for functional network identification. Neuroimage 123:11-21.

Zhang D, Snyder AZ, Shimony JS, Fox MD, Raichle ME (2010) Noninvasive functional and structural connectivity mapping of the human thalamocortical system. Cereb Cortex 20:1187-1194.

Zingg B, Hintiryan H, Gou L, Song MY, Bay M, Bienkowski MS, Foster NN, Yamashita S, Bowman I, Toga AW, Dong HW (2014) Neural networks of the mouse neocortex. Cell 156:1096-1111.

Captions to figures:

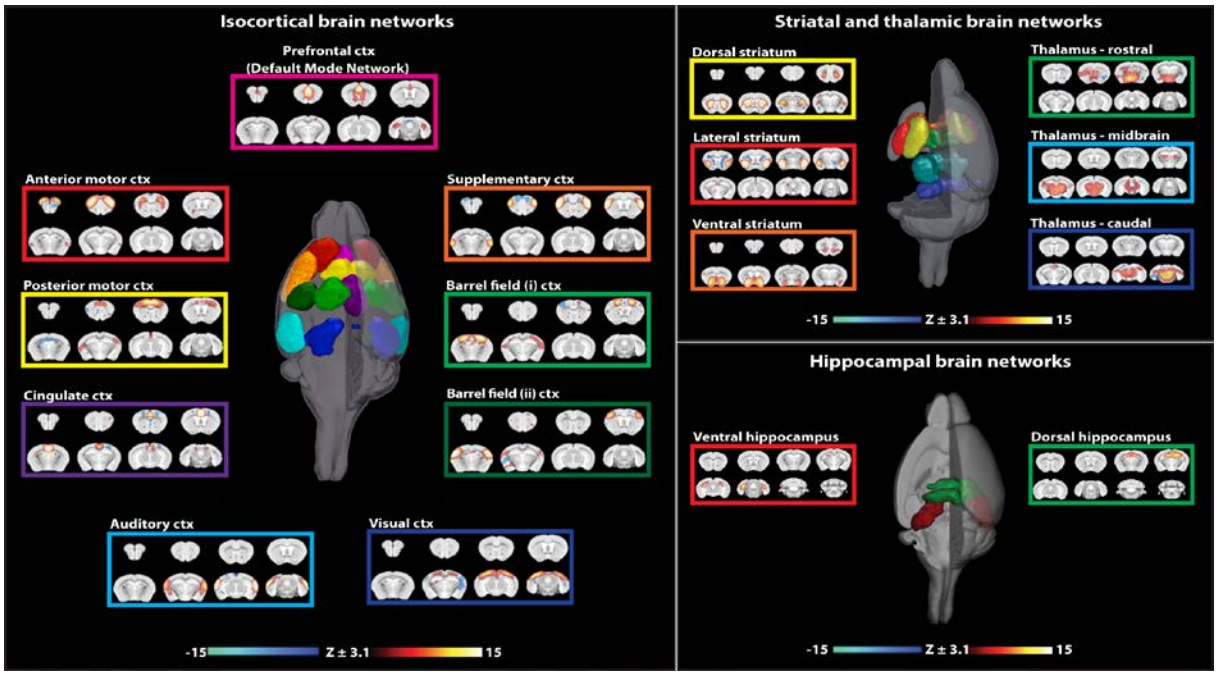

Figure 1 | Independent component analysis revealed the presence of robust resting-state networks in the mouse brain. Optimized MR acquisition, anaesthesia and handling, and image processing protocols lead to readily defined isocortical, striatal, thalamic and hippocampal rs-fMRI networks.

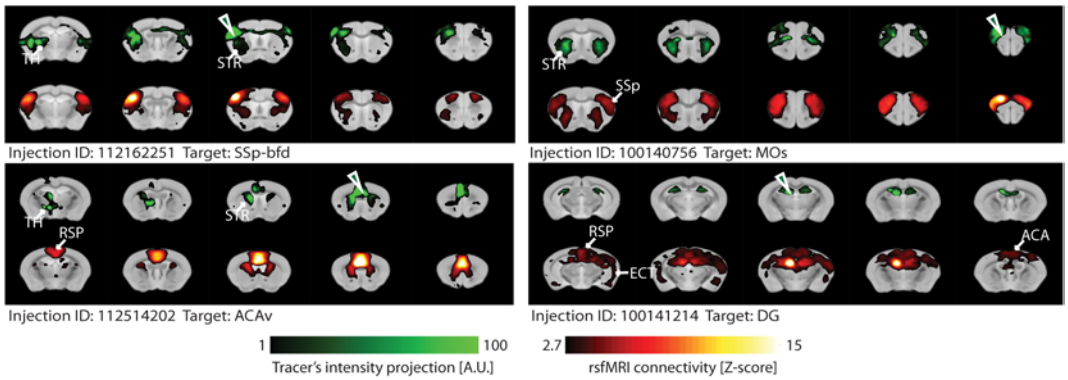

Figure 2 | Qualitative comparison between tracer distribution indicating structural connectivity (green; upper rows) and FC pattern derived from rs-fMRI (red; lower rows) for four selected injection sites/seeds. The results illustrate a high degree of similarity between the measurements, particularly in ipsilateral cortico-striatal connectivity. High overlaps were seen also in contralateral cortico-cortical and hippocampalo-hippocampal connections, while cortico-thalamic anatomical projections were not detected by rs-fMRI.

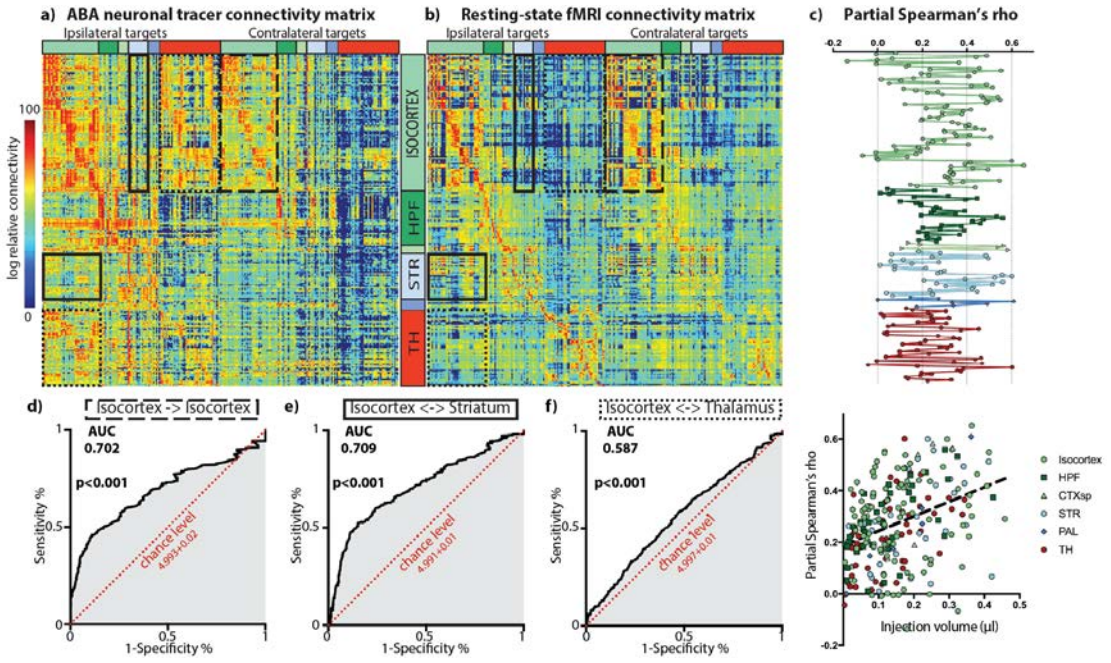

Figure 3 | Comparison of **(a)** the viral tracer connectivity matrix and **(b)** the corresponding functional connectivity matrix from 238 seed-injection sites by 254 target ROIs reveals striking similarities, in particular regarding the interactions within the isocortex. Partial Spearman's rho (corrected for target ROI volume) between structural and functional connections originating from each seed/injection experiment is displayed in (c) and show weak-to-intermediate (rho: 0.2-0.4) and average-to-strong (rho: 0.4-0.6) correlations for most of the cortical, hippocampal and striatal seeds. Conversely, we were able to detect injection areas in which the SC-FC correlation dropped to non-significant levels (rho: 0-0.2); this is notable for injections in prefrontal areas (ACAd, PL, ILA, ORBl), CA1, Striatum, Amygdala, and some thalamic nuclei and may be driven by the relatively low injected volume and by the absence of reciprocal projections between these and other brain regions. Receiver operating characteristic (ROC) curves for **(d)** isocortex → isocortex (dashed square boxes), **(e)** isocortex ↔ striatum (black square boxes), **(f)** isocortex ↔ thalamus (dotted square boxes). The area under the curve indicates the degree of similarity between the structural and functional metrics, ranging from 0.5 (chance level) to 1 (full similarity). Permutation testing confirmed the significant (>chance level distribution) agreement between SC and FC in all the macro-scale connections, with medium-to-high (>0.7) AUC levels for isocortex to its contralateral counterpart and for isocortex to striatum, and low (<0.6) for isocortical to thalamic connections.

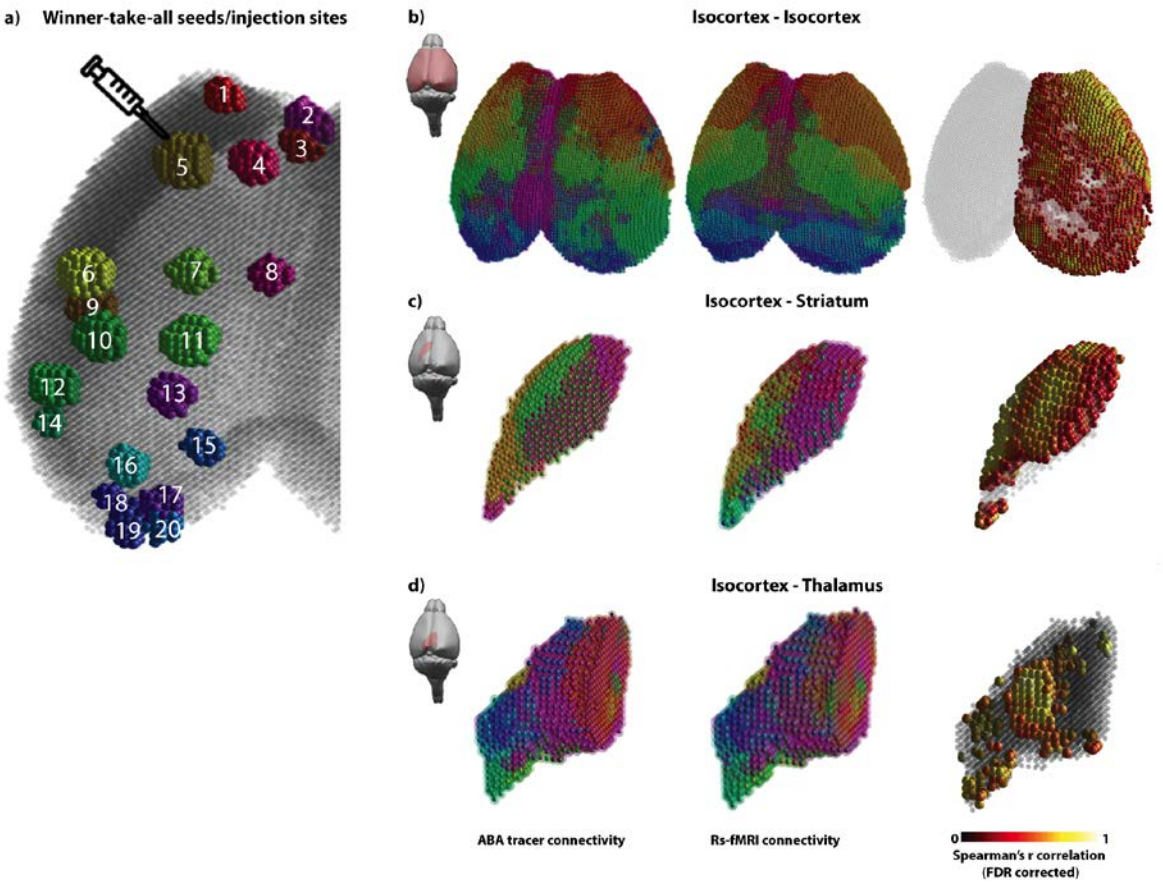

Figure 4 | Winner-takes-all analysis for 20 injection sites/seeds located in the isocortex. (a) Location of injection sites/seeds used for the winner-takes-all analysis mapped on a surface representation of the mouse isocortex. The labels are: (1) MOs, (2) ORBm, (3) PL, (4) MOs, (5) MOp, (6) SSp-bfd, (7) MOp, (8) ACAd, (9) SSs, (10) SSp-bfd, (11) SSp-ll, (12) AUDd, (13) PTLp, (14) AUDd, (15) RSPagl, (16) AUDd, (17) VISp, (18) VISp, (19) VISp, (20) VISp. Two spheres of different diameters and transparency are drawn in each voxel, indicating the first and second strongest connected injection sites/seeds originating from the isocortex toward **(b)** contralateral isocortex, **(c)** ipsilateral striatum, and **(d)** ipsilateral thalamus. Voxel-based Spearman's R correlation indicates significant correlation between tracer's injection and rs-fMRI data. Voxels from both isocortical and striatal maps present significant correlation (86.9 and 87.8% of total voxels respectively) between structural and functional connectivity. In contrast, thalamic map presents significant correlation between the two modalities in 8.8% of the voxels only, specifically in the anteroventral and ventral posteromedial nuclei of the thalamus.

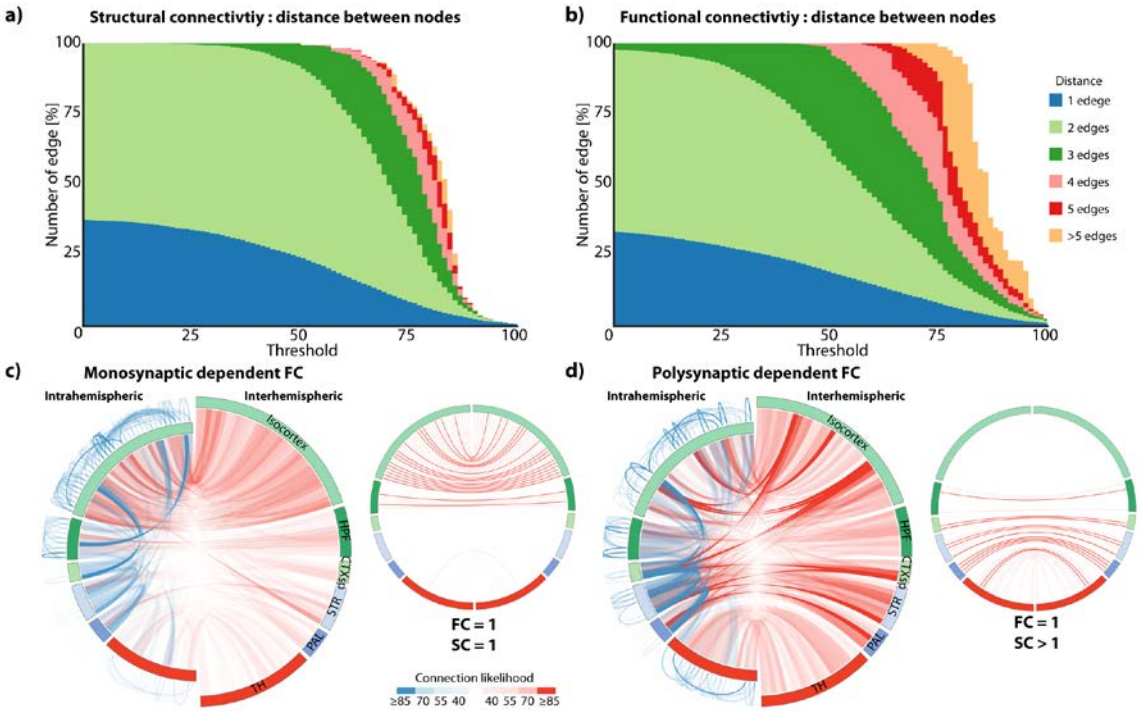

Figure 5 | Distance separating node pairs from structural and functional connectivity at varying matrix threshold revealed a similar distribution (a-b). Structural and functionally connectivity matrices were normalized to a range 0-100. Distance was computed for both matrices with incremental threshold with step size =1. At lower threshold, the number of edges separating any node pairs remains between 1 and 2 edges. The distance increases as threshold is increased. **(c,d)** Distance analysis reveals mono- or polysynaptic connectivity likelihood (CL) of functional connectivity. Large circular plots show transparency-coded links that represent CL for intra- (blue) and interhemispheric (red) connections across the brain. For sake of clarity, intrahemispheric connections within brain structures are plotted outside and inside of the circle labelling the major brain regions (left side of graphs). Smaller circular plots indicate links between bilateral homotopic region pairs only. **(c)** The isocortex presents balanced intra- and interhemispheric monosynaptic CL, towards hippocampal formation (HPF), cortical sub-plate (CTXsp), and striatum (STR) (intra-) and towards contralateral homotopic ROI (inter-). **(d)** Polysynaptic CL present more diverse links between ROIs from different ontological structures and hemispheres, e.g. STR to contralateral isocortex and STR. Polysynaptic homotopic interactions are found in the CTXsp, STR, PAL, and thalamus. Likelihood values are given in %.